The Effects of Different HITRAN Versions on Calculated Long-Wave Radiation and Uncertainty Evaluation

LU Peng[1,2,3] (卢 鹏), ZHANG Hua[3*] (张 华), and JING Xianwen[1,3] (荆现文)

1 *Chinese Academy of Meteorological Sciences, Beijing* 100081

2 *Nanjing University of Information Science & Technology, Nanjing* 210044

3 *Laboratory for Climate Studies, China Meteorological Administration, Beijing* 100081

(Received April 25, 2011; in final form December 6, 2011)

ABSTRACT

Four editions of the High Resolution Transmission (HITRAN) databases (HITRAN96, HITRAN2K, HITRAN04, and HITRAN08) are compared by using a line-by-line (LBL) radiative model in the long-wave calculation for six typical atmospheres. The results show that differences in downward radiative fluxes between HITRAN96 and HITRAN08 at the surface can reach a maximum of 1.70 W m^{-2} for tropical atmospheres. The largest difference in heating rate between HITRAN96 and HITRAN08 can reach 0.1 K day^{-1} for midlatitude summer atmosphere. Uncertainties caused by line intensity and air-broadened half-widths are also evaluated in this work using the uncertainty codes given in HITRAN08. The uncertainty is found to be 1.92 W m^{-2} for upward fluxes at the top of the atmosphere (TOA) and 1.97 W m^{-2} for downward fluxes at the surface. The largest heating rate caused by the uncertainty of line intensity and air-broadened half-width can reach 0.5 K day^{-1}. The differences in optical depths between 1300 and 1700 cm^{-1} caused by different HITRAN versions are larger than those caused by the uncertainties in intensity and air-broadened half-width. This paper suggests that there is inaccurate representation of line parameters over some spectral ranges in HITRAN and more attention should be paid to these ranges in fields such as remote sensing.

Key words: High Resolution Transmission (HITRAN), long-wave radiation, optical depth, radiative flux, heating rate

Citation: Lu Peng, Zhang Hua, and Jing Xianwen, 2012: The effects of different HITRAN versions on calculated long-wave radiation and uncertainty evaluation. *Acta Meteor. Sinica*, **26**(3), 389–398, doi: 10.1007/s13351-012-0310-1.

1. Introduction

Spectroscopic databases, which are the direct input to line-by-line (LBL) radiative-transfer models, are of great importance for the accuracy of radiative calculations (Clough et al., 1992; Clough and Iacono, 1995; Zhang, 1999; Zhang and Shi, 2000; Zhang et al., 2007). The most widely used spectroscopic database in atmospheric sciences is the High Resolution Transmission (HITRAN) database (Rothman, 2010). It is updated roughly every 4 years, incorporating the latest improvements in theoretical and experimental spectroscopy, and has already gone through several versions (e.g., HITRAN96 (Rothmanet et al., 1998), HITRAN2K (Rothmanet et al., 2003), HITRAN04 (Rothmanet et al., 2005), and HITRAN08 (Rothmanet et al., 2009)). There are also some other spectroscopic databases. The GEISA (Gestion et Etude des Informations Spectroscopiques Atmosphériques) is a computer-accessible spectroscopic database designed to facilitate accurate forward atmospheric radiative-transfer calculations using an LBL and atmospheric layer-by-layer approach. Its latest version is GEISA2009 (Jacquinet-Husson et al., 2008). The Ford Motor Company database focuses on halocarbons and non-methane hydrocarbons (Sihra et al., 2001; Gohar et al., 2004; Bravo et al., 2010). Changes in the spectroscopic databases naturally

Supported by the National Science and Technology Support Program of China (2007BAC03A01), National Natural Science Foundation of China (41075056), and National Basic Research and Development (973) Program of China (2011CB403405).

*Corresponding author: huazhang@cma.gov.cn.

affect radiative-transfer calculations.

Correlated k-distribution (CKD) models (Shi, 1981; Lacis and Oinas, 1991; Fu and Liou, 1992; Zhang et al., 2003; Li and Barker, 2005) are much faster than LBL models and have a comparable accuracy. They are currently widely used as radiation schemes in general circulation models (GCMs) (Zhang et al., 2006a, b). However, correlated-k calculations are still mainly based on the effective absorption coefficients calculated by the LBL model, so their accuracy also depends on the quality of the spectroscopic database. Although spectroscopic databases have been regularly updated to new versions, privious ones are still widely used in both radiative transfer models and GCMs. Renewing the look-up table of effective absorption coefficients in the radiation scheme is grueling work in most GCMs, so it is important to evaluate the need before proceeding.

Some researchers have studied the differences between various editions of HITRAN databases for diverse uses (Feng et al., 2007; Feng and Zhao, 2009; Fomin and Falaleeva, 2009). Pinnock and Shine (1998) compared the differences in infrared irradiance, heating rate, and radiative forcing among HITRAN86, HITRAN92, and HITRAN96. They also evaluated the uncertainty caused by differences in line strength and line width. Fomin et al. (2004) demonstrated that maximal discrepancies in radiative flux were decreased from 2.5 to 0.5 W m^{-2} from the 1992–2002 to 1996–2002 editions of HITRAN. Feng et al. (2007) and Feng and Zhao (2009) addressed the effect of changes in the HITRAN database on atmospheric remote sensing. Kratz (2008) studied the sensitivity of radiation calculations to changes in the HITRAN database from 1982 to 2004. Fomin and Falaleeva (2009) gave a simple comparison of the updated HITRAN08 with previous versions and found that different water-vapor-continuum models can make a difference of 2 W m^{-2} in the short wave.

In this paper, a more detailed comparison between the latest and previous versions of HITRAN is conducted by using an LBL model. Unlike Fomin and Falaleeva (2009), the optical depth, radiative fluxes, and heating rate are completely compared, and the line parameter statistics is added. Additionally, uncertainties from spectroscopic databases are also estimated by incorporating the uncertainty codes of line intensity and air-broadened line width. The uncertainty codes of intensity and air-broadened half-width in each line used here are compared with those of Pinnock and Shine (1998). They only used one uncertainty value for all lines. The evaluation method used here is more reasonable than theirs.

The HITRAN spectroscopic database and LBL model used in this study are introduced in Section 2. In Section 3, the differences in optical depth, radiative fluxes, and heating rate among different HITRAN versions are compared in six model atmospheres. The uncertainties of optical properties are addressed in Section 4, where the uncertainties in radiative flux and heating rate caused by the uncertainties in intensity and air-broadened half-width are also shown. Finally, a conclusion is given in Section 5.

2. The database and the radiative-transfer model

2.1 HITRAN spectroscopic database

The HITRAN spectroscopic database is widely used in atmospheric remote sensing and sounding, radiative calculations, and other fields. The latest version was released in 2008 as HITRAN08 (Rothman et al., 2009). The main information in the database includes line-transition parameters, infrared cross-sections, ultraviolet LBL parameters, cross-section, and aerosol refractive indices.

Table 1 gives a summary of line parameters in the long wave (0–3000 cm^{-1}) for five greenhouse gases and four different HITRAN versions (HITRAN96, HITRAN2K, HITRAN04, and HITRAN08). As can be seen from Table 1, the total number of lines for each gas increases every time when HITRAN is updated. For example, the total number of lines for CO_2 in HITRAN08 is four times as many as that in HITRAN04. However, the sum of line intensities and the intensity-weighted air-broadened line widths have no significant differences.

Taking CO_2 as an example, Table 2 explains why,

Table 1. Line statistics between 0 and 3000 cm^{-1}

HITRAN database	N	$\sum S$ ($cm^2 mol^{-1} cm^{-1}$)	$\sum S\alpha$ (cm^{-1})
H_2O			
2008	18429	6.388E–17	7.6826E–2
2004	18429	6.341E–17	7.8819E–2
2000	16422	6.358E–17	7.5242E–2
1996	15571	6.347E–17	7.5568E–2
CO_2			
2008	161272	1.098E–16	7.3577E–2
2004	40095	1.098E–16	7.3577E–2
2000	38843	1.098E–16	7.3577E–2
1996	38843	1.098E–16	7.3577E–2
O_3			
2008	357375	1.762E–17	7.6412E–2
2004	295292	1.761E–17	7.6399E–2
2000	258958	1.819E–17	7.2288E–2
1996	258958	1.819E–17	7.2288E–2
CH_4			
2008	153792	8.374E–18	5.832E–2
2004	129684	8.354E–18	5.858E–2
2000	37392	8.440E–18	5.916E-2
1996	37392	8.440E–18	5.916E–2
N_2O			
2008	32307	6.967E-17	7.704E–2
2004	32299	6.967E–17	7.704E–2
2000	20828	6.974E–17	7.656E–2
1996	20827	6.974E–17	7.656E–2

N is the number of total lines, $\sum S$ is the sum of line intensity, and $\sum S\alpha/\sum S$ is the intensity-weighted air-broadened line widths.

Table 2. Line statistics between 0 and 3000 cm^{-1} for CO_2 according to line intensity

CO_2	N	$\sum S(cm^2 mol^{-1} cm^{-1})$	$\sum S\alpha/\sum S(cm^{-1})$
2008			
>0	161272	1.098E–16	7.3577E–2
>1E–26	8983	6.2215E–18	7.3980E–2
>1E–22	505	6.1921E–18	7.3985E–2
>1E–18	0	0	0
2004			
>0	40095	1.098E–16	7.3577E–2
>1E–26	30071	1.0849E–16	7.3697E–2
>1E–22	1959	1.0839E–16	7.3669E–2
>1E–18	34	8.3164E–17	7.3940E–2
1996			
>0	38843	1.098E–16	7.3577E–2
>1E–26	30708	1.098E–16	7.3577E–2
>1E–22	1978	1.097E–16	7.3579E–2
>1E–18	34	8.316E–17	7.3940E–2

with the total line number increasing, the sums of the line intensities and intensity-weighted air-broadened line widths show little change. The line parameters for CO_2 are classified by line intensity in Table 2. In HITRAN96 and HITRAN2K, the sum of line intensities is almost entirely a function of lines with intensities greater than 10^{-26} cm^2 mol^{-1} cm^{-1}. However, these strong lines make up only 6% of the overall line intensities in HITRAN08. This means that there are many more weak lines in HITRAN08 than in previous versions. Because of their dominant 94% contribution to the total line intensity, these weak lines are very important to radiation calculations.

2.2 LBL model

In this study, we use an LBL model called ZS2000 (Zhang, 1999; Zhang and Shi, 2000; Zhang et al., 2007, 2008). Compared with the LBLRTM (Line-By-Line Radiative Transfer Model) (Clough et al., 2005), the relative differences in upward and downward radiative fluxes of ZS2000 are less than 3.1%, and the absolute differences in heating rates are less than 0.13 K day^{-1} (Zhang et al., 2005). To calculate the absorption coefficient, the following line parameters are taken from the HITRAN database, i.e., transition wave number, intensity, air-broadened half-width, self-broadened half-width, lower-state energy, and temperature-dependence exponent of air-broadened half-width.

The formula for calculating line intensity is (Zhang, 1999; Zhang and Shi, 2000)

$$S(T) = S(T_s)\frac{Q_v(T_s)Q_r(T_s)}{Q_v(T)Q_r(T)} \cdot \exp\left[\frac{1.439E''(T-T_s)}{TT_s}\right], \quad (1)$$

where $S(T)$ is the line intensity for any temperature, $S(T_s)$ is the line intensity under standard conditions, E'' is the lowest-state energy, and Q_v and Q_r are functions of vibration and rotation, respectively (both of which depend on temperature). When the temperate ranges between 175 and 325 K, Q_v can be fitted by the following formulas for different gases (Zhang, 1999; Zhang and Shi, 2000)

$$H_2O : Q_v(T) = 1.00486 - (4.41322 \times 10^{-5})T + (9.73170 \times 10^{-8})T^2, \quad (2)$$

$$CO_2 : Q_v(T) = 1.05385 - (8.11142 \times 10^{-4})T + (3.18772 \times 10^{-6})T^2, \quad (3)$$

$$O_3 : Q_v(T) = 1.06712 - (7.74561 \times 10^{-4})T + (2.36961 \times 10^{-6})T^2, \tag{4}$$

$$N_2O : Q_v(T) = 1.05746 - (9.09125 \times 10^{-4})T + (3.86439 \times 10^{-6})T^2, \tag{5}$$

$$CH_4 : Q_v(T) = 1.00486 - (4.41322 \times 10^{-5})T + (9.73170 \times 10^{-8})T^2, \tag{6}$$

$$Q_r(T) = (T/T_s)^j. \tag{7}$$

Here, for H_2O, O_3, and CH_4, $j = 1.5$; and for CO_2 and N_2O, $j = 1.0$. The absorption coefficient is obtained from

$$k_\nu = \frac{k_0 Y}{\pi} \int_{-\infty}^{\infty} \frac{\exp(-t^2)}{Y^2 + (x-t)^2} \mathrm{d}t, \tag{8}$$

where k_ν is the absorption coefficient at wavenumber ν, $k_0 = S/(\alpha_D\sqrt{\pi})$, $x = (\nu - \nu_0)/\alpha_D$, $Y = \alpha_L/\alpha_D$, α_L and α_D are the Lorentz and Doppler half widths, respectively, ν is the position of the line, and ν_0 is the center of the line position. Using quantum mechanics, we find

$$\alpha_D = \nu_0/c(2KT/m)^{1/2} = (4.301 \times 10^{-7})\nu_0\sqrt{T/M}, \tag{9}$$

$$\alpha_L(P,T) = \alpha_L(P_0,T_0)(P/P_0)(T/T_0)^{-n}, \tag{10}$$

where K is the Boltzmann constant, m is molecular mass, c is light speed, T is temperature, P is pressure, M is the molecular weight, and n is the temperature-dependent exponent of air-broadened half-width.

Six model profiles representing typical atmospheric conditions are adopted in this study, i.e., tropical (TRO), midlatitude summer (MLS), midlatitude winter (MLW), sub-arctic summer (SAS), sub-arctic winter (SAW), and United States Standard (USS) (McClatchey et al., 1972). The resolution of ZS2000 is 0.01 cm^{-1}, with a single line cut-off of 5 cm^{-1}. The vertical model atmosphere from 0 km at the surface to 100 km at the TOA is divided into 100 uniform layers. As non-local thermodynamic equilibrium should be considered above 70 km, only the results below 70 km are analyzed. The concentrations of water vapor and ozone are obtained directly from the six profiles, whereas those of CO_2, CH_4, and N_2O are set to constant values of 386.8, 1.803, and 0.3225 ppmv, respectively, according to the 2009 Greenhouse Gas Bulletin (http://www.wmo.int/pages/prog/arep/gaw/ghg/GHGbulletin.html).

3. Effects of different HITRAN versions on the radiation calculation

3.1 Optical-depth

The optical-depth formula is

$$\tau_\nu(z_1, z_2) = \int_{z_1}^{z_2} k_\nu \rho(z) \mathrm{d}z, \tag{11}$$

where τ_ν is the optical depth at wavenumber ν, z_1 and z_2 are the two heights along the light path, k_ν is the absorption coefficient at ν, and $\rho(z)$ is the density depending on height z.

Since there is no large difference in the optical depths of the five major greenhouse gases among the six atmospheric profiles, Fig. 1 only shows the optical depth of the five major greenhouse gases under MLS conditions, along with the relative differences between the previous HITRAN versions and HITRAN08. The spectral resolution is 5 cm^{-1}. The differences between HITRAN versions are obvious (Fig. 1). The largest relative error between HITRAN04 and HITRAN08 ranges from 490 to 600 cm^{-1}, with a high relative difference of 17.99% at 497.5 cm^{-1}. The relative difference between the HITRAN2K and HITRAN08 peaks ranges from 2500 to 2820 cm^{-1}, with a high relative difference of 99%. The most significant relative differences between HITRAN96 and HITRAN08 are in the range 2390–2430 and 780–920 cm^{-1}, with an extremely large value of 44.23% at 2412.5 cm^{-1}. HITRAN96 and HITRAN2K are different only in the H_2O absorption bands. Figure 1 also shows that, in the range of 2500–2820 cm^{-1}, the relative difference between HITRAN96 and HITRAN08 is smaller than that between HITRAN2K and HITRAN08, but the reverse is true in the range 780–920 cm^{-1}. This means that HITRAN96 may be better than HITRAN2K for band 2500–2820 cm^{-1}, whereas HITRAN2K may be superior to HITRAN96 for band 780–920 cm^{-1} for the H_2O line parameters.

3.2 Radiative fluxes and heating rate

Table 3 shows the calculated upward fluxes at the TOA and downward fluxes at the surface, putting the HITRAN line parameters into ZS2000 for five major greenhouse gases and six atmospheric conditions, as

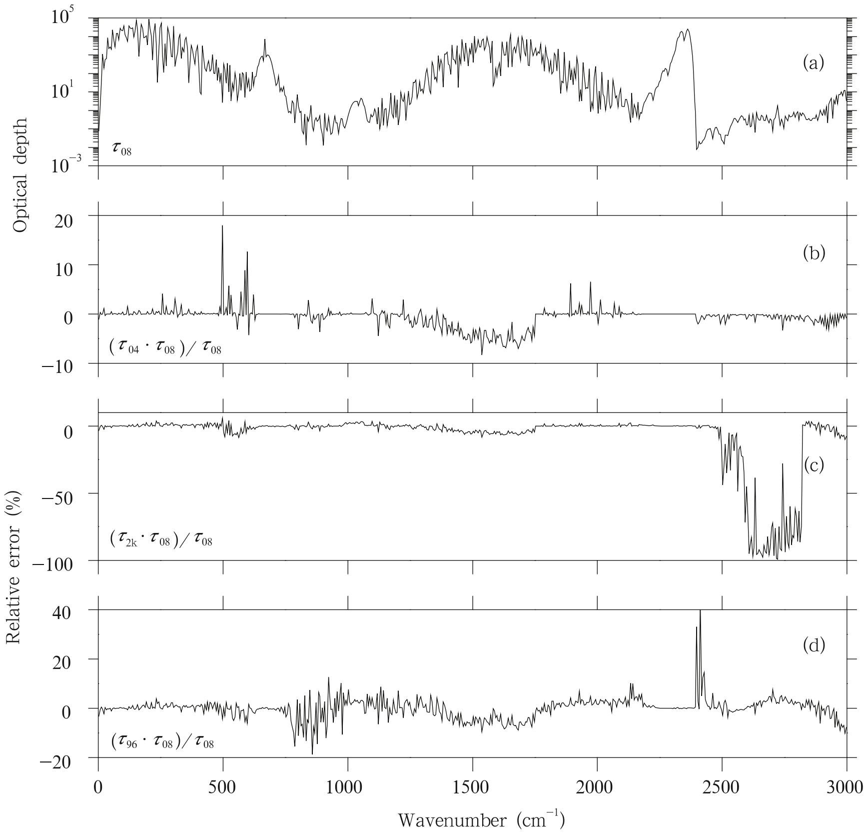

Fig. 1. Comparison of optical depth in the long-wave regime from 0 to 3000 cm^{-1} for MLS atmosphere. All the curves have been smoothed to have a 5-cm^{-1} resolution. (a) The optical depth calculated by HITRAN08; the relative difference between (b) HITRAN04 and HITRAN08, (c) HITRAN2K and HITRAN08, and (d) HITRAN96 and HITRAN08.

well as the differences between earlier versions and HITRAN08. The difference in downward fluxes between HITRAN08 and HITRAN96 is larger than 1.07 W m^{-2} for TRO, MLS, and SAS. In TRO, the maximum difference is 1.70 W m^{-2}. At the TOA, the differences are typically less than 0.28 W m^{-2} for all six atmospheric profiles. The major differences between HITRAN96 and HITRAN08 occur for downward rather than upward radiation. The differences between HITRAN04/HITRAN2K and HITRAN08 are 0.48 W m^{-2} at most for all six atmospheric profiles at both the TOA and the surface, which is smaller than those between HITRAN96 and HITRAN08. This highlights the tremendous improvement of this database since 1996.

Figure 2 shows the heating rate for the MLS atmosphere. The heating rate difference between HITRAN08 and HITRAN04 is less than 0.05 K day^{-1}. Difference between HITRAN08 and HITRAN96 could be larger than 0.1 K day^{-1}. The largest

Table 3. Comparison of radiative fluxes (W m^{-2}) from 0 to 3000 cm^{-1} for six typical atmospheres

	HITRAN08		HITRAN04–HITRAN08		HITRAN2K–HITRAN08		HITRAN96–HITRAN08	
	$F^{\uparrow}$	$F^{\downarrow}$	$F^{\uparrow}$	$F^{\downarrow}$	$F^{\uparrow}$	$F^{\downarrow}$	$F^{\uparrow}$	$F^{\downarrow}$
TRO	297.06	332.85	–0.24	0.12	–0.17	0.01	0.28	–1.70
MLS	286.89	303.96	–0.24	0.21	–0.19	0.08	0.15	–1.38
MLW	232.30	204.38	–0.18	0.48	–0.17	0.32	–0.01	–0.48
SAS	269.04	268.18	–0.22	0.34	–0.18	0.16	0.13	–1.07
SAW	199.97	156.49	–0.12	0.48	–0.12	0.39	–0.05	–0.16
USS	265.23	262.52	–0.25	0.40	–0.21	0.21	0.09	–0.85

$F^{\uparrow}$ is the upward radiative flux at the TOA and $F^{\downarrow}$ is the downward radiative flux at the surface.

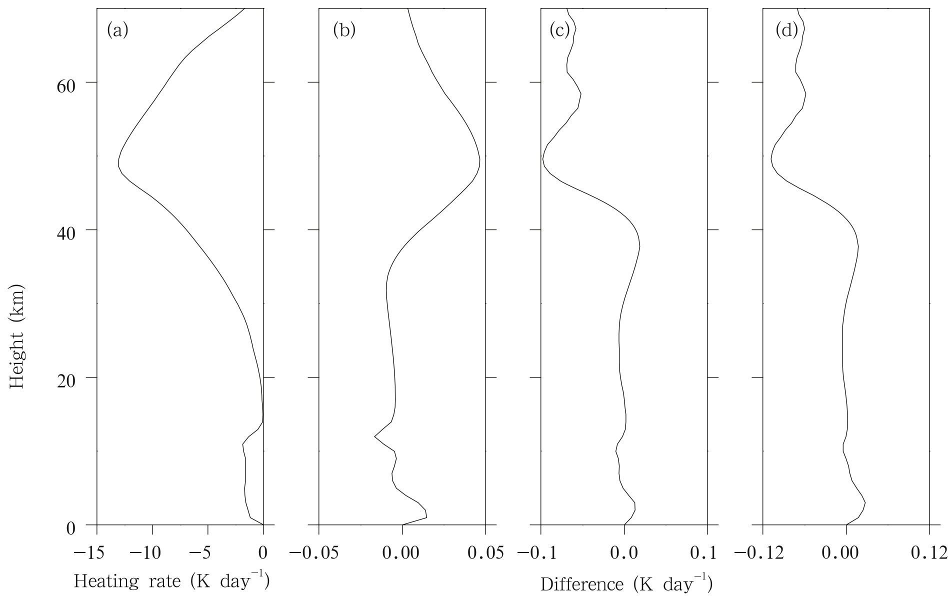

Fig. 2. Heating rate calculated by HITRAN08 and the differences of heating rates between other HITRAN versions and HITRAN08 for MLS atmosphere. (a) The heating rate calculated by HITRAN08; the relative difference between (b) HITRAN04 and HITRAN08, (c) HITRAN2K and HITRAN08, and (d) HITRAN96 and HITRAN08.

differences are all at the height of 50 km, and the heating rates in the stratosphere are dominated by the 15-micron CO_2 band. This suggests that most of the differences at 50 km come from the differences in the CO_2 line parameter among different HITRAN versions. The heating rate calculated by HITRAN08 is about 0.05 K day^{-1} smaller than that using HITRAN04, but about 0.1 K day^{-1} larger than that using HITRAN2K and HITRAN96. This means that the CO_2 absorption calculated by HITRAN08 is smaller than that calculated by HITRAN04, but larger than that using HITRAN96/HITRAN2K.

4. Uncertainty evaluation

The uncertainties in optical properties, radiative fluxes, and heating rates caused by the intensity and air-broadened half-width are estimated in this section using the uncertainty codes of intensity and air-broadened half-width from HITRAN08. Table 4 lists the uncertainty codes from Rothman et al. (2005). The uncertainty codes of intensity and air-broadened half-width are added for most lines as line parameters in HITRAN04. They are only provided for a few molecules and a few bands in some previous cases. To quantitatively estimate the uncertainties in optical properties, radiative fluxes, and heating rates, uncertainty codes of intensity and air-broadened half-width in each line are used here. The uncertainty values are taken to be in the middle of the uncertainty range when the uncertainty codes are larger than 3. For example, the uncertainty value is set to 7.5% when the code equals 5, and 20% when the code equals 3. When the codes are less than 3, a mean of all uncertainty values for codes more than 2 is used. Table 5 shows the line-number statistics with the same uncertainty code for both intensity and air-broadened half-width

Table 4. Uncertainty codes adopted by HITRAN (Rothman et al., 2005)

Code	Intensity, air-broadened half-width
0	Unreported or unavailable
1	Default or constant
2	Average or estimate
3	$\geqslant$ 20%
4	$\geqslant$ 10% and $<$ 20%
5	$\geqslant$ 5% and $<$ 10%
6	$\geqslant$ 2% and $<$ 5%
7	$\geqslant$ 1% and $<$ 2%
8	$<$ 1%

Table 5. Line statistics with the same uncertainty code in intensity and air-broadened half-width

Code		0	1	2	3	4	5	6	7	8
H_2O	Intensity	3604	0	0	0	1	14150	131	543	0
	Half-width	123	0	0	0	2525	13336	1628	615	202
CO_2	Intensity	87	0	3804	12539	112440	19686	12683	18	15
	Half-width	0	0	0	0	8791	152481	0	0	0
O_3	Intensity	158721	0	0	13196	75814	93335	14829	1480	0
	Half-width	15724	0	61	0	83453	120325	137812	0	0
N_2O	Intensity	451	0	0	0	0	293	31422	141	0
	Half-width	0	168	0	0	0	0	32139	0	0
CH_4	Intensity	0	0	0	78005	16932	52942	5912	0	0
	Half-width	0	0	76766	50919	15394	8506	2050	157	0

in HITRAN08 for five greenhouse gases. It is more reasonable than the method given by Pinnock and Shine (1998), as they used only one uncertainty value for all lines.

From Eqs. (8) and (11), we know that optical depth is positively correlated with intensity. Pinnock and Shine (1998) showed that for a line of finite opacity, an increase in line width will transfer opacity from the line center to the line wings, increasing the total ability of the gas to absorb and emit. There is a major correlation between air-broadened half-width and optical depth for a single line. They also showed that the upward flux decreases as the optical depth increases, whereas the downward flux increases as the optical depth increases. Therefore, when the intensity and air-broadened half-width both reach the lower limit of uncertainty, maximum upward fluxes at the TOA and minimum downward fluxes at the surface are implied

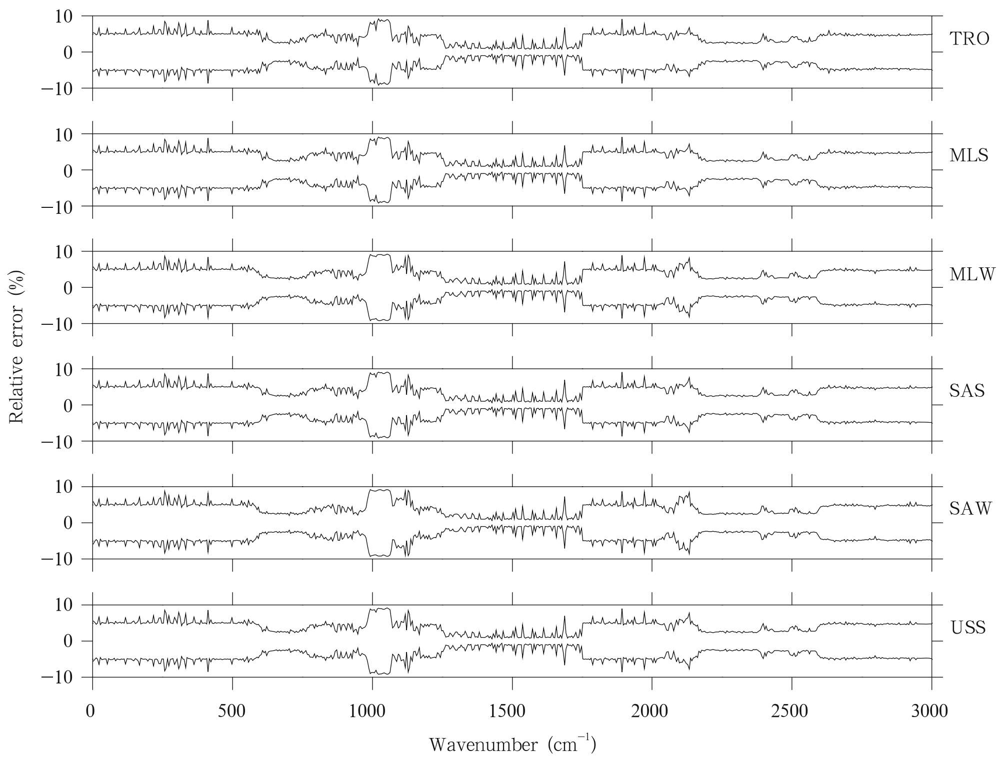

Fig. 3. Uncertainties of optical depth for six typical atmospheres. Top to bottom panels are for tropical (TRO), midlatitude summer (MLS), midlatitude winter (MLW), sub-arctic summer (SAS), sub-arctic winter (SAW), and United States Standard (USS) atmospheric profiles, respectively.

theoretically. In fact, as for each single line, the upper and lower limits of uncertainties caused by intensity and air-broadened half-width are not always reached simultaneously. It seems impossible for all lines in the spectral region to reach the limits simultaneously. Thus, the uncertainties we describe here are theoretical and far larger than the true values.

Figure 3 shows the uncertainty of optical depth calculated by the method described above. It suggests that the uncertainties are always less than 10% in long wave. Comparing Fig. 1 with Fig. 3, we can see that the differences caused by different HITRAN versions can surpass those caused by uncertainty of intensity and air-broadened half-width in some regions (for example, in the range from 1300 to 1700 cm^{-1}). This suggests that there is inaccuracy in the representation of some spectral ranges by HITRAN and more attention should be paid to these ranges in fields such as remote sensing.

Table 6 shows the values of radiative flux uncertainty calculated using the uncertainty codes of intensity and air-broadened half-width. The biggest absolute uncertainties in the upward flux at the TOA and the downward flux at the surface are 1.92 and 1.97 W m^{-2} (both for TRO).

Figure 4 shows the differences in heating rates caused by uncertainties in intensity and air-broadened half-width for the six atmospheric profiles. The largest uncertainties all appear at heights of about 50 km for the six atmospheres, which are similar for different HITRAN versions. This suggests that most of the uncertainties at 50 km come from the uncertainty in intensity and air-broadened half-width of CO_2. The largest heating rate uncertainty is about 0.5 K day^{-1} for USS.

Table 6. Values of radiative flux uncertainty calculated using the uncertainty codes of intensity and air-broadened half-width

	HITRAN08		Uncertainty (W m^{-2})	
	$F^{\uparrow}$	$F^{\downarrow}$	$F^{\uparrow}$	$F^{\downarrow}$
TRO	297.06	332.85	[–1.82, 1.92]	[–1.97, 1.86]
MLS	286.89	303.96	[–1.63, 1.73]	[–1.91, 1.79]
MLW	232.30	204.38	[–1.10, 1.16]	[–1.69, 1.59]
SAS	269.04	268.18	[–1.34, 1.43]	[–1.84, 1.75]
SAW	199.97	156.49	[–0.76, 0.80]	[–1.51, 1.42]
USS	265.23	262.52	[–1.52, 1.61]	[–1.85, 1.78]

5. Conclusions

First, the line parameters in different HITRAN versions are compared and it is seen that the added lines in HITRAN08 are mostly weak. These additional weak lines are either new or come from splitting of strong lines. By analyzing the CO_2 line number and line strength, we find that the splitting of strong lines makes a major contribution.

Then, the differences in optical depth, radiative fluxes, and heating rate among different versions of HITRAN are studied in the long-wave regime for five greenhouse gases and six model atmospheres using the LBL model of ZS2000. The relative errors in optical depth could be larger than 90% in some spectral ranges. Based on these, we find that the maximum difference of downward radiative flux at the surface can reach 1.7 W m^{-2} between HITRAN96 and HITRAN08 for tropical atmospheres. The differences among HITRAN08, HITRAN04, and HITRAN2K are no larger than 0.48 W m^{-2} for the six atmospheres at both the TOA and the surface. The differences are relatively smaller than those between HITRAN96 and HITRAN08. The differences of water-vapor heating rates between HITRAN08 and HITRAN04 are all less than 0.05 K day^{-1} for all levels of the MLS atmosphere; those between HITRAN08 and other versions can be larger than 0.1 K day^{-1}.

Finally, the uncertainty codes of intensity and air-broadened half-width from HITRAN08 are used to evaluate the uncertainty of optical properties, radiative flux, and heating rate caused by the intensity and air-broadened half width. It is seen that the uncertainties are mostly less than 1.92 W m^{-2} for the upward radiative fluxes at the TOA and less than 1.97 W m^{-2} for the downward radiative fluxes at the surface. The maximum uncertainty in heating rate reaches 0.5 K day^{-1} at a height of 50 km for the USS atmosphere.

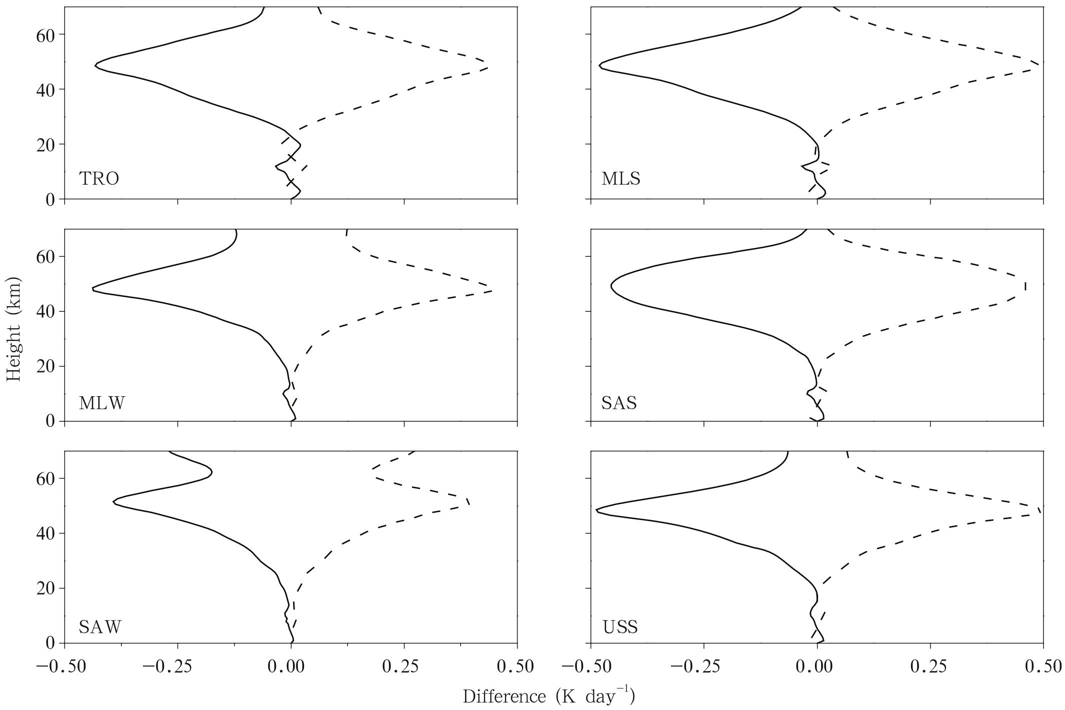

Fig. 4. As in Fig. 3, but for heating rate. Solid lines represent the bias caused by the minimum value of the uncertainty of intensity and air-broadened half-width, and dashed lines denote the bias caused by the maximum value of them.

REFERENCES

Bravo, I., A. Aranda, M. D. Hurley, et al., 2010: Infrared absorption spectra, radiative efficiencies, and global warming potentials of perfluorocarbons: Comparison between experiment and theory. *J. Geophys. Res.*, **115**, D24317, doi:10.1029/2010JD014771.

Clough, S. A., M. J. Iacono, and J. L. Moncet, 1992: Line-by-line calculation of atmospheric fluxes and cooling rates: Application to water vapor. *J. Geophys. Res.*, **97**, 15761–15785.

——, and ——, 1995: Line-by-line calculations of atmospheric fluxes and cooling rates. Part II: Application to carbon dioxide, ozone, methane, nitrous oxide, and the halocarbons. *J. Geophys. Res.*, **100**, 16519–16535.

——, M. W. Shephard, E. J. Mlawer, et al., 2005: Atmospheric radiative transfer modeling: A summary of the AER codes, short communication. *J. Quant. Spectrosc. Radiat. Transfer*, **91**, 233–244.

Feng Xuan, Zhao Fengsheng, and Gao Wenhua, 2007: Effect of the improvement of the HITRAN database on the radiative transfer calculation. *J. Quant. Spectrosc. Radiat. Transfer*, **108**, 308–318.

——, and ——, 2009: Effect of changes of the HITRAN database on transmittance calculations in the near-infrared region. *J. Quant. Spectrosc. Radiat. Transfer*, **110**, 247–255.

Fomin, B. A., T. A. Udalova, and E. A. Zhitnitskii, 2004: Evolution of spectroscopic information over the last decade and its effect on line-by-line calculations for validation of radiation codes for climate models. *J. Quant. Spectrosc. Radiat. Transfer*, **86**, 73–85.

——, and V. A. Falaleeva, 2009: Recent progress in spectroscopy and its effect on line-by-line calculations for the validation of radiation codes for climate models. *Atmospheric and Oceanic Optics*, **22**, 626–629.

Fu Qiang and Liou Kuonan, 1992: On the correlated k distribution method for radiative transfer in non-homogeneous atmospheres. *J. Atmos. Sci.*, **49**, 2139–2156.

Gohar, L. K., G. Myhre, and K. P. Shine, 2004: Updated radiative forcing estimates of four halocarbons. *J. Geophys. Res.*, **109**, 01107–01109.

Jacquinet-Husson, N., N. A. Scott, A. Chedin, et al., 2008: The GEISA spectroscopic database: Current and future archive for earth and planetary atmosphere studies. *J. Quant. Spectrosc. Radiat. Transfer*, **109**, 1043–1059.

Kratz, D. P., 2008: The sensitivity of radiative transfer calculation to the changes in the HITRAN database from 1982 to 2004. *J. Quant. Spectrosc. Radiat. Transfer*, **109**, 1060–1080.

Lacis, A. A., and V. A. Oinas, 1991: A description of the correlated k distribution method for modeling nongray gaseous absorption, thermal emission and multiple scattering in vertically inhomogeneous atmospheres. *J. Geophys. Res.*, **96**, 9027–9063.

Li Jiangnan, and H. W. Barker, 2005: A radiation algorithm with correlated-k distribution. Part 1: Local thermal equilibrium. *J. Atmos. Sci.*, **62**, 286–309.

McClatchey, R. A., R. W. Fenn, J. E. Selby, et al., 1972: Optical Properties of the Atmosphere. Optical Physics Laboratory, Air Force Cambridge Research Laboratories, 1–108.

Pinnock, S., and K. P. Shine, 1998: The effects of changes in HITRAN and uncertainties in the spectroscopy on infrared irradiance calculations. *J. Atmos. Sci.*, **55**, 1950–1964.

Rothman, L. S., 2010: The evolution and impact of the HITRAN molecular spectroscopic database. *J. Quant. Spectrosc. Radiat. Transfer*, **111**, 12–13.

——, C. P. Rinsland, A. Goldman, et al., 1998: The HITRAN molecular spectroscopic database and HAWKS (HITRAN atmospheric workstation): 1996 edition. *J. Quant. Spectrosc. Radiat. Transfer*, **60**, 665–710.

——, A. Barbe, D. C. Benner, et al., 2003: The HITRAN molecular spectroscopic database: Edition of 2000 including updates through 2001. *J. Quant. Spectrosc. Radiat. Transfer*, **82**, 5–44.

——, D. Jacquemart, A. Barbe, et al., 2005: The HITRAN 2004 molecular spectroscopic database. *J. Quant. Spectrosc. Radiat. Transfer*, **96**, 139–204.

——, I. E. Gordon, and A. Barbe, 2009: The HITRAN 2008 molecular spectroscopic database. *J. Quant. Spectrosc. Radiat. Transfer*, **110**, 533–572.

Shi Guangyu, 1981: An accurate calculation and representation of the infrared transmission function of the atmospheric constituents. Ph. D. dissertation, Tohoku University, Japan, 191 pp.

Sihra, K., M. D. Hurley, K. P. Shine, et al., 2001: Updated radiative forcing estimates of 65 halocarbons and nonmethane hydrocarbons. *J. Geophys. Res.*, **106**(D17), 20493–20506.

Zhang Hua, 1999: On the study of a new correlated k-distribution method for nongray gaseous absorption in the inhomogeneous scattering atmosphere. Ph.D. dissertation, Institute of Atmospheric Physics, Beijing, China, 169 pp. (in Chinese)

—— and Shi Guangyu, 2000: A fast and efficient line-by-line algorithm on atmospheric absorption. *Chinese J. Atmos. Sci.*, **24**(1), 111–121. (in Chinese)

——, Nakajima, T., Shi Guangyu, et al., 2003: An optimal approach to overlapping bands with correlated k-distribution method and its application to radiative calculations. *J. Geophys. Res.*, **108**, 4641–4653.

——, Shi Guangyu, and Liu Yi, 2005: A comparision between the two line-by-line integration algorithms. *Chinese J. Atmos. Sci.*, **29**(4), 581–593. (in Chinese)

——, ——, T. Nakajima, et al., 2006a: The effects of the choice of the k-interval number on radiative calculations. *J. Quant. Spectrosc. Radiat. Transfer*, **98**, 31–43.

——, T. Suzuki, T. Nakajima, et al., 2006b: Effects of band division on radiative calculations. *Optical Engineering*, **45**(1), 016002–016010.

——, Shi Guangyu, and Liu Yi, 2007: The effects of line-wing cutoff on radiative calculations. *Acta Meteor. Sinica*, **65**(6), 968–975. (in Chinese)

——, ——, and ——, 2008: The effects of line-wing cutoff on radiative calculations. *Acta Meteor. Sinica*, **22**(2), 248–255.